JOURNAL OF GEOPHYSICAL RESEARCH, VOL. 112, D10S04, doi:10.1029/2006JD007578, 2007

Atmospheric in situ measurement of nitrate radical (NO_3) and other photolysis rates using spectroradiometry and filter radiometry

H. Stark,[1,2] B. M. Lerner,[1,2] R. Schmitt,[3] R. Jakoubek,[1] E. J. Williams,[1,2] T. B. Ryerson,[1] D. T. Sueper,[1,2] D. D. Parrish,[1] and F. C. Fehsenfeld[1,2]

Received 30 May 2006; revised 12 February 2007; accepted 20 March 2007; published 22 May 2007.

[1] We describe field measurements of nitrate radical photolysis rates, $j(NO_3)$, conducted during the International Consortium for Atmospheric Transport and Transformation (ICARTT) study in the summer of 2004 in the northeastern United States on board the NOAA research vessel *Ronald H. Brown* (*RHB*) and the NOAA aircraft *WP-3*. The photolysis rates of 17 other atmospherically important compounds were also measured. Direct measurements of spectral actinic fluxes using spectroradiometers were conducted on board the *WP-3*, which were then converted into photolysis rates. On board *RHB*, we used filter radiometers that specifically measured $j(NO_3)$ and were calibrated before and after the campaign by the spectroradiometers. NO_3 photolysis rates ranged from below the detection limit of 10^{-5} s^{-1} at twilight to peak values of 0.5 s^{-1} over clouds at midday. The measurement uncertainties were 9% for the spectroradiometers and 14% for the filter radiometers. A field intercomparison between ship and aircraft instruments showed general agreement, indicating that aircraft data can be used to calculate the ship nadir radiation from the ocean surface. The measurements were used to evaluate the importance of photolysis of nitrate radicals in the troposphere. One result was that because of its spatial correlation with NO, NO_3 daytime loss is dominated by reaction with NO in the free troposphere and the marine boundary layer. The tropospheric branching ratio between the two NO_3 photolysis channels producing NO and NO_2, was found to be (10.8 ± 1.2)% for NO in the lower troposphere.

Citation: Stark, H., B. M. Lerner, R. Schmitt, R. Jakoubek, E. J. Williams, T. B. Ryerson, D. T. Sueper, D. D. Parrish, and F. C. Fehsenfeld (2007), Atmospheric in situ measurement of nitrate radical (NO_3) and other photolysis rates using spectroradiometry and filter radiometry, *J. Geophys. Res.*, *112*, D10S04, doi:10.1029/2006JD007578.

1. Introduction

[2] The measurement of photolysis rates is essential in understanding atmospheric radical chemistry. The photolysis rate, j, of a certain photolytic process is defined as the first-order loss rate coefficient (in units of s^{-1}) due to radiation:

(R1) $$AB + h\nu \rightarrow A + B$$

$$j = -\frac{1}{[AB]}\frac{d[AB]}{dt} \quad (1)$$

It is calculated by integrating the product of the spectral actinic flux, $F(\lambda)$, the quantum yield of the molecule, $\Phi(\lambda)$, and its absorption cross section, $\sigma(\lambda)$, over the wavelength, λ:

$$j = \int F(\lambda) \cdot \Phi(\lambda) \cdot \sigma(\lambda) d\lambda \quad (2)$$

[3] The spectral actinic flux, F, is defined as the number of photons of a certain wavelength reaching a unit area independent of direction per unit time per spectral interval. It is commonly expressed in photons cm^{-2} s^{-1} nm^{-1}. The wavelength-dependent unitless quantity quantum yield, $\Phi(\lambda)$, is the probability for the specified photolytic process. More details of basic physical and chemical processes related to radiation are given by *Hofzumahaus* [2006].

[4] In this paper we will focus on the measurement of photolysis rates for the nitrate radical (NO_3) which has recently gained attention through the development of in situ instruments and their deployment in the field [*Brown et al.*, 2001; *Simpson*, 2003; *Wood et al.*, 2005]. Nitrate radical is an important oxidant in the atmosphere [*Wayne et al.*, 1991; *Winer et al.*, 1984]. Photolysis and reaction with nitric oxide (NO) are the most significant daytime loss processes for NO_3. Together, they prevent the existence of large NO_3 mixing ratios during daytime, making nitrate radicals particularly important during nighttime. However, at twilight periods during the evening and the morning, and occasion-

[1] Chemical Sciences Division, Earth System Research Laboratory, NOAA, Boulder, Colorado, USA.
[2] Also at Cooperative Institute for Research in Environmental Sciences, University of Colorado, Boulder, Colorado, USA.
[3] Metcon, Inc., Boulder, Colorado, USA.

0148-0227/07/2006JD007578$09.00

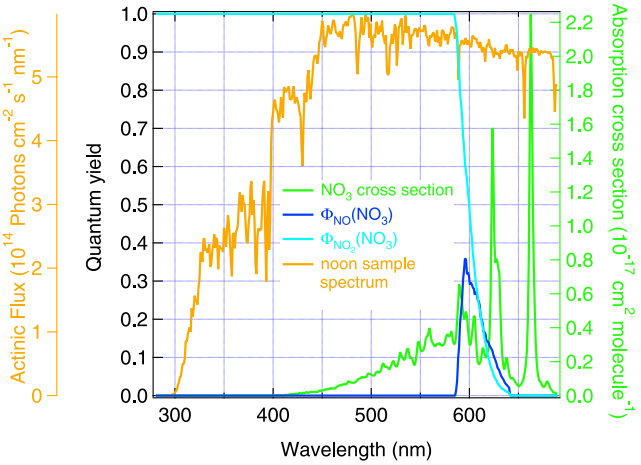

Figure 1. NO_3 spectrum, quantum yield for NO production from NO_3 photolysis (R1), quantum yield for NO_2 production (R2), sample midday actinic flux, measurement taken on clear day of 15 July 2004 at 5200 m altitude over the North Atlantic Ocean at 40°N and 65°W with a solar zenith angle of 18.5°. See legend for identification of the traces.

ally during midday under low light conditions, significant nitrate mixing ratios can exist. *Geyer et al.* [2003] have outlined the conditions under which daytime nitrate can occur. Recently, two studies have been published evaluating the importance of daytime nitrate radical occurrence [*Brown et al.*, 2005; *Osthoff et al.*, 2006], which included the $j(NO_3)$ measurements described in this publication. Measurements of nitrate radical photolysis from different instruments have been reported from a study in a deciduous forest in Germany during the ECHO campaign in 2002 and 2003 [*Bohn*, 2006]. The authors report $j(NO_3)$ values on the order of 0.2 s^{-1}. Model calculations give a midday, clear-sky photolysis rate of around 0.2 s^{-1}, equal to an NO_3 lifetime of 5 s [*Magnotta and Johnston*, 1980].

[5] The nitrate radical absorbs light in the visible spectral region. It has significant absorption cross sections from 420 to 690 nm. It is photolyzed via two channels, producing either NO or NO_2:

$$(R2) \qquad NO_3 + h\nu \rightarrow NO + O_2$$

$$(R3) \qquad \rightarrow NO_2 + O(^3P)$$

Figure 1 shows the NO_3 absorption spectrum and quantum yields for (R2) and (R3) from *Sander et al.* [2006]. A typical summer midday actinic flux spectrum measured at 5 km altitude during ICARTT 2004 is also included in Figure 1.

2. Experimental Details

[6] We used two types of instruments to measure photolysis rates for NO_3 and other compounds. Wavelength-resolved spectroradiometers measured actinic fluxes, from which we calculated photolysis rates. Integrating filter radiometers measured individual photolysis rates after calibration with spectroradiometers.

[7] The first section of this chapter will describe the spectroradiometers, the optical receptors for light collection, the optical fibers for light transport and the calibration procedures. The second section will describe setup and calibration of the filter radiometers.

2.1. Spectroradiometers

[8] The nitrate radical (NO_3) is photodissociated in the troposphere at wavelengths between 420 and 640 nm. We used two spectroradiometers to cover this wavelength range, one for the ultraviolet/visible range (UV/VIS) and one for the visible range (VIS). The combination of two spectroradiometers allowed measurements with higher wavelength resolution, which is especially important for photolysis rates of compounds with highly structured absorption spectra in the ultraviolet other than NO_3, for example formaldehyde.

2.1.1. UV/VIS Spectroradiometer

[9] The UV/VIS spectroradiometer measured radiation from 280 to 490 nm and was also used for measuring photolysis rates of 17 other atmospherically important compounds besides NO_3. Table 1 shows all photolysis rates calculated from actinic fluxes measured with the UV/VIS spectroradiometer. Also included in Table 2 are campaign average and maximum photolysis rates for these compounds measured on board the *WP-3* during ICARTT 2004. A complete description of conditions encountered during ICARTT 2004 is given by *Fehsenfeld et al.* [2006]. Some details on the range of temperatures, pressures, locations, and solar zenith angles encountered are given in the results section. Solar zenith angles encountered during the campaign ranged between minimum values of 10° and over 100° at night. The instrument is based on a commercial dual-grating spectrometer with charge-coupled device (CCD) array. The incoming light passes through a 100 μm slit, is dispersed by 2 gratings of unequal ruling density (to avoid reentrant light) and then imaged onto a back-thinned CCD array with 1340 horizontal and 400 vertical pixels [Princeton Instruments SP-150, Trenton, New Jersey, USA]. Sets of 16 vertical pixels were binned (summed) in the instrument to increase data transfer rates. A rotating 2-slot blade driven by a precision stepper motor set the exposure time to 0.5 s and the measurement frequency to 1 Hz. The advantage of this setup is faster acquisition of full spectra compared to scanning a monochromator. Therefore photolysis rates at a 1 Hz measurement cycle are available.

[10] Scattered, diffuse light within the instrument cannot be fully suppressed in a non-wavelength-scanning spectroradiometer and needs to be accounted for to achieve accurate signal levels. At 294 nm, the atmospheric actinic flux is zero for all altitudes encountered with the spectroradiometer. We used the signal at this wavelength as the average scattered light signal, set the signal below that wavelength to zero and subtracted this value from all other wavelengths. Figure 2 shows signals before and after scattered light subtraction for typical midday clear-sky conditions. We have previously performed measurements using optical filters blocking different parts of the spectrum to investigate the wavelength-dependence of the scattered light. This wavelength dependence of the scattered light had a negligible influence on the actinic flux due to the steep decrease of the actinic

Table 1. Photolysis Rates Determined From Actinic Flux Measured With UV/VIS and VIS Spectroradiometer[a]

Compound	Average j, s^{-1}	Maximum j, s^{-1}	Spectrum	Quantum Yields
Acetone	5.0×10^{-7}	3.3×10^{-6}	1	2
HCHO	5.6×10^{-5}	2.9×10^{-4}	3	3
CH_3CHO	4.1×10^{-6}	2.7×10^{-5}	1	3, 4
CH_3OOH	3.8×10^{-6}	1.9×10^{-5}	3	5
Glyoxal	5.5×10^{-5}	2.6×10^{-4}	3	3
H_2O_2	4.7×10^{-6}	2.4×10^{-5}	5	6
HNO_2	1.4×10^{-3}	6.9×10^{-3}	5	3
HNO_3	4.1×10^{-7}	2.1×10^{-6}	5	6
HNO_4 (UV)	3.0×10^{-6}	1.7×10^{-5}	5	3
Methacrolein	3.9×10^{-6}	1.9×10^{-5}	7	7
Methylethylketone	8.2×10^{-6}	4.5×10^{-5}	1	3
Methylglyoxal	7.8×10^{-5}	3.7×10^{-4}	8, 9	8
Methylvinylketone	3.8×10^{-5}	2.2×10^{-5}	7	7
N_2O_5	2.9×10^{-5}	1.3×10^{-4}	5	5
NO_2	6.5×10^{-3}	3.1×10^{-2}	5	10
NO_3	1.8×10^{-1}	6.9×10^{-1}	6	6
O_3	2.1×10^{-5}	1.2×10^{-4}	6	6
PAN	4.7×10^{-7}	2.3×10^{-6}	11	6

[a]Campaign average values from *WP-3* aircraft during ICARTT 2004 show typical values for these photolysis rates, and maximum values indicate possible enhancements by clouds. References are as follows: 1, *Martinez et al.* [1992]; 2, *McKeen et al.* [1997]; 3, *Atkinson et al.* [1997]; 4, *Horowitz et al.* [1982]; 5, *DeMore et al.* [1997]; 6, *Sander et al.* [2006]; 7, *Gierczak et al.* [1997]; 8, *Staffelbach et al.* [1995]; 9, *Meller et al.* [1991]; 10, *Gardner et al.* [1987]; 11, *Talukdar et al.* [1995].

flux in the ultraviolet. Scattered light is only a significant fraction (>10%) of the overall signal at UV wavelengths below 303 nm. Therefore the assumption that the scattered light is constant gives accurate results for most measured photolysis rates, because most measured compounds have relatively small photolysis rates below this wavelength. An exception is $j(O(^1D))$, which has significant photolysis rates (between 20 and 30%) at this wavelength. Calculations of $j(O(^1D))$ conducted with and without subtraction of scattered light resulted in differences of up to 6% of the total photolysis rates. These deviations can be regarded as maximum uncertainties for $j(O(^1D))$ due to imprecise scattered light subtraction. For the wavelengths important for NO_3 photolysis (420–490 nm), scattered light is negligibly small. It should be noted that the scattered light amounts from the UV/VIS spectroradiometer are significantly lower than encountered in single-grating CCD instruments, which could be more than an order of magnitude above the signal at wavelengths under 300 nm, as, e.g., described by *Edwards and Monks* [2003].

Table 2. Uncertainties for $j(NO_3)$ From Spectroradiometers and Filter Radiometers[a]

	Uncertainty, %
Spectroradiometers	
Wavelength calibration	1
FEL lamps	1
Field standards	3
Lamp-head distance	0.4
Zenith angle dependence	3
Cross-talk	2
Slit function	0.8
Detector nonlinearity	1.4
Total instrumental	5
Literature spectra and quantum yields	7
Total spectroradiometers	9
Filter radiometers	
Error from spectroradiometers	9
Calibration	10
Estimation of upwelling radiation	3
Total	14

[a]Combined uncertainties are derived using quadratic error propagation.

2.1.2. VIS Spectroradiometer

[11] We used a single-grating spectroradiometer for measuring actinic fluxes from 460 to 690 nm. The light passing through a 100 μm entrance slit is collimated, dispersed by the grating and imaged onto a 1024 horizontal by 256 vertical pixel CCD array [Acton Research INS 150-250 B, Acton, Massachusetts, USA]. As with the UV-VIS spectroradiometer, sets of 16 vertical pixels were binned before being transferred to a computer. An electrically controlled mechanical shutter was used to set the light exposure time on the CCD array to 100 ms at a measurement frequency of 1 Hz.

[12] The spectrometer was aligned to measure light from about 450 to 697 nm. To be able to subtract the scattered light background, which is typically below 1% of the signal,

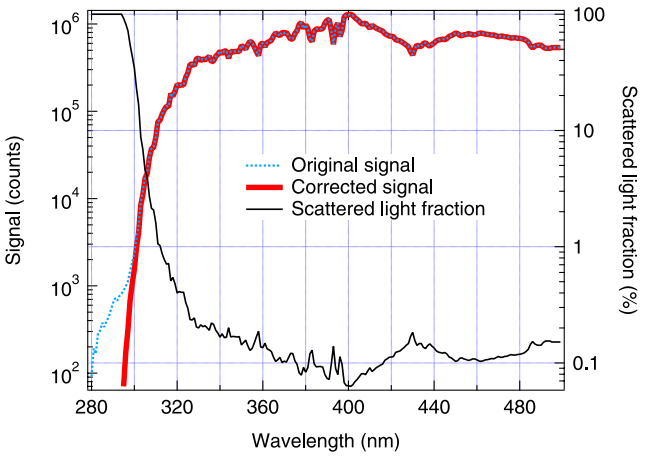

Figure 2. Scattered light removal from UV/VIS spectroradiometer. Dotted curve indicates original signal, solid thin curve indicates scattered light fraction, and solid thick curve indicates corrected signal. Signal was measured on clear-sky conditions on 15 July 2004 at 5000 m altitude over the North Atlantic Ocean at 42°N and 66°W with a solar zenith angle of 35°.

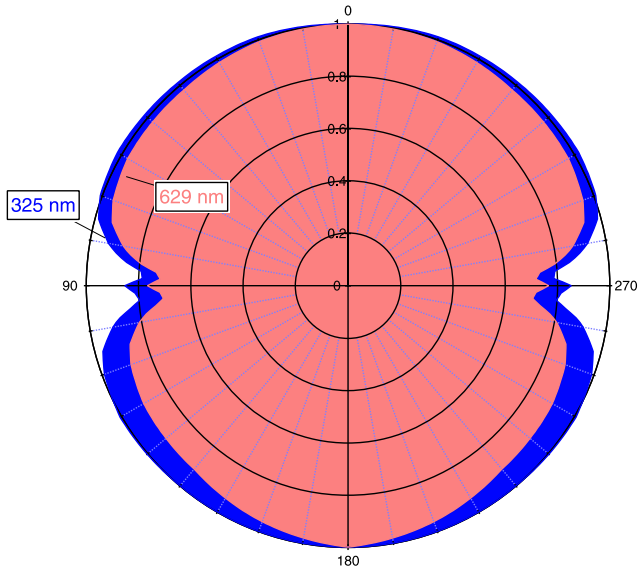

Figure 3. Zenith angle dependence Z_p of spectroradiometer response (normalized) at two wavelengths: 325 nm (outer polar graph) and 629 nm (inner polar graph).

we inserted a GG475 band pass filter behind the entrance slit in order to block out light below 460 nm. As with the UV/VIS spectroradiometer, scattered light measurements using different band pass filters gave no indication of a possible wavelength dependence of the scattered light. We used an average of the first 20 horizontal pixels of the raw signal (≈450–456 nm, the band pass filter's transmittance is below 3×10^{-5} at these wavelengths) as a constant scattered light amount that we subtracted from all wavelength signals. We reported data from this spectrometer for the wavelength range 460–690 nm.

2.1.3. Light Receptors

[13] The light receptors must give a signal independent of the incident light angle to accurately measure actinic fluxes. Triple-layered, sand-blasted quartz domes [Metcon Inc., Boulder, Colorado, USA] are used to achieve this angle-independence. The quartz domes are mounted in aluminum cylinders to be able to have sufficient sealing of the domes against ambient air. A drying tube is mounted to the sealed cylinders to avoid condensation. These receptor heads are a modification of the design by *Volz-Thomas et al.* [1996], which itself was a modification of heads described by *Junkermann et al.* [1989]. A combination of two light receptors, one facing up (zenith head) and one facing down (nadir head) collected light from 4π steradians. Each head-only collected light from one hemisphere. To achieve this, the heads are mounted in the center of flat discs (shadow rings) at a depth designed to block out light from angles larger than 90° from both the zenith and the nadir. The shadow rings are flat aluminum discs of 30 cm diameter, painted flat black. A small lip of 5 mm height on the outside of the ring provides a well defined shadow on the shadow ring at high zenith angles. This design is a modification of the shadow ring described by *Shetter and Muller* [1999] We determined the azimuth and zenith angle dependencies of the receptors by laboratory measurements. These measurements were conducted in a calibration box to remove the influence of room lights or scattered light. The box consisted of two cubic chambers of about 2 m^3 volume that were separated by a wall with an aperture built into the center of the wall. The inside of each chamber was covered with black velvet cloth to reduce the amount of light scattering from the walls. We rotated each receptor mounted in the shadow ring at a distance of about 50 cm from a constant halogen light source. The exact distance of the receptors to the light source was determined by assuming an equivalent plane receiver, as described by *Hofzumahaus et al.* [1999] The diameter of the circular aperture in the wall between the chambers was adjusted to fully illuminate the receptors and the shadow ring while avoiding any light on the chamber walls. The receptor signal did not depend strongly on the azimuth angle (<3% change over 360°), and was also independent of the zenith angle up to about 75°. The signal decreased above this angle to about 50% at 90° and 0% at 105° zenith angle. Thus, when the signals of both nadir and zenith heads are combined, referred to as the angular response Z_p, approximately 100% of the incoming light is measured at each angle. Figure 3 shows a polar plot of Z_p as a function of the zenith angle for two wavelengths, 325 and 629 nm. The signal deviates from unity for zenith angles between 75 and 105 degrees and is generally smaller at 629 nm. Unfortunately, this deviation could not be removed by different receptor-shadow ring alignments. There have been several studies investigating correction possibilities for the nonideal zenith angle dependence in ground based and airborne studies [*Hofzumahaus et al.*, 1999, 2002; *Jakel et al.*, 2005]. The angular response function Z_p can be used to calculate correction factors Z_h for the nonideal behavior of the combination of the two measurement heads:

$$Z_h = \alpha \cdot Z_p(\vartheta) + \frac{1-\alpha}{2\pi}\int_{UH} Z_p(\omega)d\omega + \frac{\beta}{2\pi}\int_{LH} Z_p(\omega)d\omega \quad (3)$$

The functions α and β are defined by:

$$\alpha = \frac{F_0}{F_0 + F\downarrow} \quad \text{and} \quad \beta = \frac{F\uparrow}{F_0 + F\downarrow}, \quad (4)$$

where F↑ is the diffuse upwelling, F↓ the diffuse downwelling, and F_0 the direct downwelling actinic flux. UH and LH refer to the upper and lower hemisphere, respectively.

[14] We calculated correction factors Z_h, normalized to the ideal case of $Z_p = 1$, under the assumption of isotropic diffuse radiation ($\alpha = 0$). The factors Z_h as a function of wavelength are shown in Figure 4. The dependence on β is small and does not change Z_h significantly; the calculation is limited by low light intensities at short wavelengths. A fourth-order polynomial was fit to these data. This correction function is only valid for isotropic diffuse radiation. In the case of diffuse nonisotropic or direct radiation, correction factors can be different. We decided to correct all data by the isotropic diffuse correction factors shown in Figure 4 by dividing the actinic fluxes by the fit to the measured Z_h function. We did not further analyze the data sets collected during this study in terms of the influence of different amounts of upwelling radiation or direct downwelling radiation. The application of the correction function resulted in increased upward welling photolysis rates of 2% for compounds absorbing in the ultraviolet (e.g., O_3, NO_2,

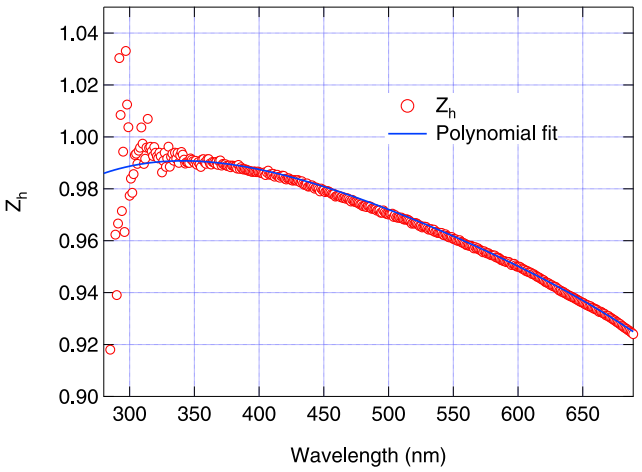

Figure 4. Correction function Z_h for combined zenith and nadir heads as a function of wavelength (markers). Curve indicates fourth-order polynomial fitting function for Z_h.

H_2CO) and 4% for $j(NO_3)$. A remaining uncertainty of 3% was estimated to account for diffuse nonisotropic or direct radiation.

2.1.4. Optical Fibers

[15] We used commercial optical quartz fiber bundles [Ceramoptec, East-Longmeadow, Massachusetts, USA] with 36 fibers per bundle and a fiber thickness of 200 μm to deliver the light to the spectroradiometers. The fibers were attached to the optical center of each light receptor (zenith and nadir). To be able to supply light to both spectroradiometers from both receptors, each bundle was split in half and then combined with half from the other receptor. The zenith and nadir head fibers were arranged vertically parallel to the entrance slits of the spectroradiometers such that the upper half of the slit would collect light from fibers from the zenith head and the lower half fibers from the nadir head.

2.1.5. Calibration Measurements

[16] The light collected by the receptors, transmitted by the fibers and dispersed by the gratings, results in a signal on the CCD arrays, where the horizontal pixel number is proportional to the wavelength and the signal strength (counts) is proportional to the light intensity at a certain wavelength. We conducted calibration measurements for both spectroradiometers to convert the pixel number into wavelength and the counts into actinic flux. The wavelength calibration was accomplished by a combination of Hg and Cd emission lines from atomic lamps and solar radiation using a literature sunlight spectrum [*Delbouille et al.*, 1973]. During field missions, sections of the measured spectra were fitted to Fraunhofer lines always present in the sunlight. These fits were conducted for the first 60 s every 10 min. All measured spectra were shifted by the offsets to literature line positions. For the UV/VIS spectrometer two Fraunhofer lines at 393.4 and 396.8 nm (Ca H- and K-lines) served as calibration lines, whereas one line at 656.3 nm (H_α-C line) was used for correcting spectra from the VIS spectrometer.

[17] Calibrated halogen lamps supplied the standard for the intensity scale. These NIST-traceable FEL standard lamps have lifetimes in excess of 100 hours and their intensity fluctuates less than 0.4% per 10 hours [*Harrison et al.*, 2000]. We conducted calibration measurements for each receptor in the laboratory to establish the intensity scales for the spectroradiometers. In the field, we monitored the consistency of the calibration with commercial halogen lamps that were calibrated in the laboratory against the FEL standard lamps. Calibrations were performed by covering one receptor to block out any stray light onto the CCD. These measurements also allowed an estimate of possible cross talk between the heads. For the nadir head, a maximum amount of 0.6% stray light was determined for the UV/VIS spectrometer and of 0.8% for the VIS spectroradiometer. With a maximum ratio of downward to upward flux of 10:1, these cross talk amounts can result in increased nadir signals of up to 6% for the UV/VIS spectroradiometer and up to 8% for the VIS spectroradiometer. The cross-talk amounts for the zenith head were slightly higher, with a maximum of 1.2% for the UV/VIS and 2.3% for the VIS spectroradiometer. However, total fluxes will be less influenced, since ratios of upward over downward fluxes reached maximum values of 90% in clouds, resulting in maximum enhancements for the zenith head of 1.3 and 2.6% for the UV/VIS and VIS spectroradiometer, respectively. The influence of the cross-talk for total fluxes can reach values of up to 1.1% for the UV/VIS and 2.2% for the VIS spectroradiometer. These values can be seen as upper limits for cross-talk errors of the photolysis rates, since they are maximum values reached at certain wavelengths.

[18] A computer algorithm converted the measured wavelength-resolved actinic fluxes, integrated to 1-nm resolution, from both spectroradiometers into photolysis rates for the two NO_3 photolysis channels $j_{NO}(NO_3)$ (R2), $j_{NO_2}(NO_3)$(R3), and for atmospheric photolysis channels for 17 other compounds (see Table 1). We used temperature-dependent absorption cross sections and quantum yields from *Sander et al.* [2006]. Figure 1 shows the NO_3 absorption spectrum and quantum yields at 298 K.

2.2. Filter Radiometers

[19] In addition to the spectroradiometers, we used commercial filter radiometers manufactured by Metcon Inc. [Boulder, Colorado, USA] to specifically measure NO_3 photolysis rates. Filter radiometers use a combination of optical band pass filters to match the NO_3 action spectrum (product of absorption spectrum and quantum yield) and photodiodes to measure the transmitted intensity, which ideally is directly proportional to the photolysis rate. The filter/detector combination is mounted into the optical center of the same type of light receptors as used for the spectroradiometers. Figure 5 shows the combined filter and photodiode response spectrum, as measured by Metcon Inc. [Boulder, Colorado, USA], and compares it to the NO_3 literature action spectrum.

[20] To test the quality of the filter combination, we used a variety of actinic flux spectra measured by the spectroradiometers under different light conditions and calculated two sets of NO_3 photolysis rates. One set used the NO_3 action spectrum, the other set used the measured filter/photodiode combination spectrum. The agreement between the two sets was within 1%, after applying the calibration factor (see below). Hence the difference in shapes between the filter/photodiode combination spectra and the NO_3

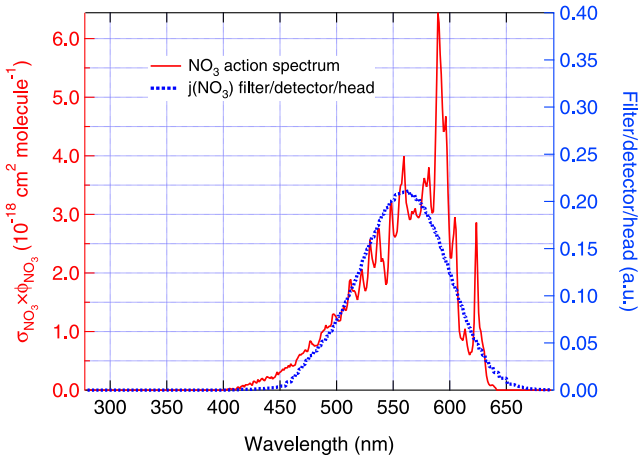

Figure 5. Comparison between NO_3 action spectrum from summed photolysis channels (R1) and (R2) (solid) and combined filter/photodiode/head response spectrum (dotted).

action spectrum is not a large source of uncertainties in the filter radiometer.

[21] Data from the spectroradiometers calibrated the filter radiometers with a series of measurements to convert the photodiode output voltage into photolysis rates. The filter radiometer and the spectroradiometer heads were facing upward next to each other and operated continuously for several days. Calibration factors were retrieved by linearly correlating the measured voltages with the NO_3 photolysis rates, derived from the measured actinic fluxes. Figure 6 shows two sets of these calibrations, one on a cloudy day, and one on a clear, sunny day. Note that the steep decline in the afternoon on the clear day is due to the early local sunset at 66° solar zenith angle caused by mountains to the west of the observation area.

[22] The overall agreement is very good with a correlation factor R^2 of 0.999. A small deviation can be seen on the clear day that may be due to either small temperature fluctuations in the photodiode sensitivity or direct-sun-angle dependences of the receptors due to inhomogeneities of the quartz diffuser domes. We did not temperature-control the $j(NO_3)$ filter radiometers, therefore sensitivity fluctuations in the photodiodes caused by temperature changes could not be ruled out, but were not addressed specifically. Further work will be conducted to temperature-control the filter radiometers. For now, these deviations were treated as uncertainties (see next section).

3. Error Estimation

3.1. Uncertainties

3.1.1. Spectroradiometers

[23] There are several factors that contribute to the overall error in the determination of NO_3 photolysis rates. These factors can be subcategorized into instrument and literature uncertainties. Significant instrument uncertainties are wavelength and intensity calibration, zenith angle dependencies, geometrical imprecision, cross-talk, slit-function effects, and detector nonlinearity. Table 2 summarizes these uncertainties. The error in $j(NO_3)$ from uncertainties in the instrument wavelength calibration is rather small because of the small flux fluctuations in the wavelength region important for NO_3 in combination with a relatively broadly structured NO_3 action spectrum. We estimate an error of approximately 1% from a maximum wavelength fluctuation of 1 nm. The intensity calibration uncertainty is combined from uncertainties in the FEL calibration lamp (1%) and fluctuations in the field calibration lamps (3%). The uncertainty arising from uncertainties in the distance between the FEL lamps and the measurement heads (±1 mm) accounts for 0.4%. The largest instrumental error is from the nonideal zenith-angle dependence of the light receptors. Since these receptors are designed for optimum performance in the ultraviolet spectral region, effects such as light diffraction and diffusion inhomogeneities of visible light in the quartz domes are mainly responsible for the angle dependence. As described above, the values for the nadir receptor were adjusted by a wavelength-dependent correction factor; a remaining uncertainty of 3% was estimated. An additional uncertainty of 2% arises from the cross-talk signals.

[24] A further uncertainty can arise from the slit function of the spectrometer. The solar actinic flux is measured at a fairly low resolution (full width at half maximum, FWHM = 0.9 nm). An uncertainty may arise from this lower resolution, since high-resolution structure in the actinic flux combined with high-resolution absorption spectra may result in different photolysis rates than measured. For structured spectra like formaldehyde, this effect can account to differences of up to 0.8% when integrated over the measured wavelength range. This value was calculated from combining a high-resolution ($\Delta\lambda = 0.01$ nm) solar emission spectrum [*Delbouille et al.*, 1973] with a high-resolution ($\Delta\lambda = 0.025$ nm) formaldehyde absorption spectrum [*Meller and Moortgat*, 2000] and comparing the integral of these high-resolution spectra with the integral of convoluted instrument-resolution spectra. It was incorporated as a maximum uncertainty for all photolysis rates.

[25] The two separate spectroradiometers are overlapping in the wavelength region 480–490 nm, which can be used for a consistency check. Throughout the course of the ICARTT 2004 campaign, a mean deviation of 4% was observed. Several factors contribute to this deviation. The

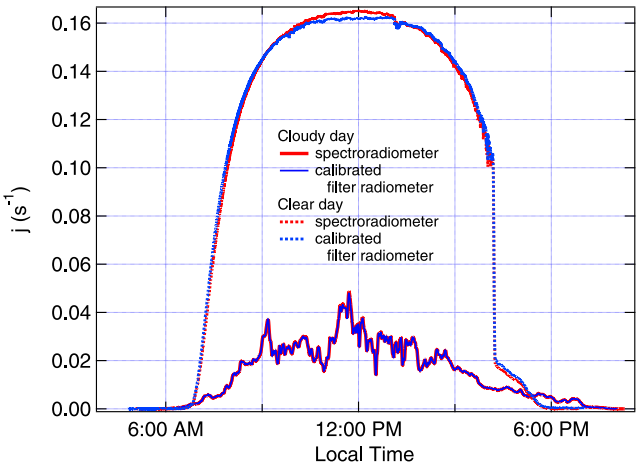

Figure 6. Calibration measurements for filter radiometers with spectroradiometers. Dotted curve indicates clear day, and solid curve indicates cloudy day.

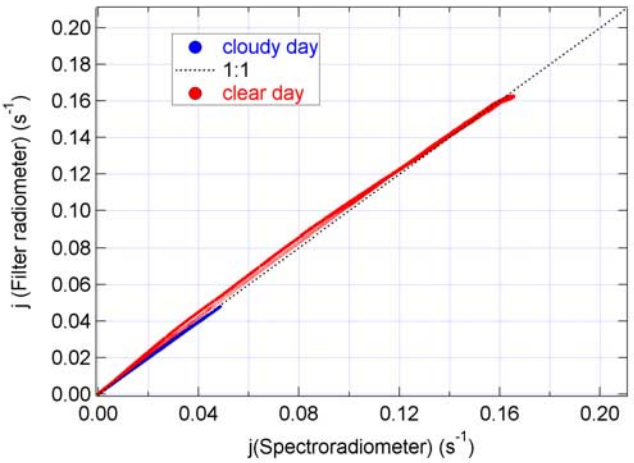

Figure 7. Correlation of filter radiometer versus spectroradiometer measurements on clear and cloudy day (markers): $R^2 = 0.999$, and line indicates 1:1 correlation.

spectra from both spectroradiometers were not measured at the exact same time. This caused fluctuations, especially during cloudy conditions. Second, wavelength uncertainties of up to 0.5 nm due to different wavelength calibrations occurred, which can also contribute to the uncertainties between the instruments. Further, the deviation showed a slight signal dependence, with 2% deviation at low and 4% deviation at high signal levels. This signal dependence is an indication of the nonlinearity of both detectors combined. We derived an additional instrument uncertainty of 1.4% through quadratic error propagation from this nonlinearity. The remaining deviation of 2% lies within the respective instrument uncertainties. All instrument uncertainties can be combined to a total instrument uncertainty of 5% using quadratic error propagation.

[26] There are additional uncertainties from literature both in the NO_3 absorption cross section and in the NO_3 quantum yield. A recent evaluation states a 7% uncertainty at the peak of the NO_3 spectrum at 662 nm [*Sander et al.*, 2006]. The total quantum yield for NO_3 photolysis only has a significant error around the transition region around 600 nm, where it drops rapidly from 1 to 0. Since the photolysis spectrum is integrated to yield the photolysis rates, uncertainties in the quantum yield do not contribute significantly.

[27] These uncertainties from literature can be combined with the instrument uncertainties to a total uncertainty of 9% for $j(NO_3)$ measured by the spectroradiometers (see Table 2).

3.1.2. Filter Radiometers

[28] Uncertainties for the filter radiometers result from the uncertainties in the spectroradiometers combined with uncertainties during the calibration measurements. Figure 7 shows the correlation plots from the calibration measurements shown in Figure 6. This correlation is much closer to 1:1 on the cloudy day, a typical result for calibration of the filter radiometers. Therefore direct sun effects on the clear day are likely to be the reason for the deviations seen on that day. Inhomogeneities in the quartz domes are the most likely cause of such deviations, although temperature fluctuations caused by radiative heating of the filter radiometers cannot be ruled out. The largest deviations were about 10% on the clear day, which was used as the overall uncertainty for the calibration measurements. An additional uncertainty of 3% arises from the estimation of the upwelling radiation. More details can be found in the results section below. Table 2 summarizes these uncertainties, which yield a total uncertainty of 14% for the filter radiometers.

3.2. Detection Limits

[29] At dark conditions at night, the standard deviation of the electrical noise of the CCD chips in the spectroradiometers and the photodiodes in the filter radiometers determine the lower detection limits for the photolysis rates. After investigating night data for aircraft and ship, we derived conservative common detection limits of 1×10^{-5} s^{-1} that were larger than 3 σ of the noise for $j(NO_3)$ from filter and spectroradiometers. This value is equivalent to an NO_3 photolytic lifetime of about 28 hours, sufficiently low for conditions encountered in most parts of the atmosphere.

4. Results and Discussion

[30] In the following sections, we will describe some results from the 2004 ICARTT measurement campaign, especially an intercomparison between the two types of instruments installed on the *WP-3* airplane and the *Ronald H. Brown* research vessel. We were also able to determine the atmospheric branching ratio between the two NO_3 photolysis channels. Further, we will discuss the importance of photolysis as an NO_3 loss during daytime and the importance of NO_3 photolysis as a source of catalytic destruction of tropospheric ozone.

4.1. The 2004 ICARTT Data Set

[31] The instruments were deployed on two platforms during the International Consortium for Atmospheric Transport and Transformation (ICARTT) study during the summer of 2004 in the northeastern United States. The spectroradiometers were integrated into the NOAA *WP-3* aircraft that was stationed in Portsmouth, New Hampshire and conducted 16 research flights between 5 July and 15 August. The filter radiometers were installed on board the NOAA research vessel *Ronald H. Brown* (*RHB*), approximately 18 m above waterline, and measured $j(NO_3)$ continuously from 5 July to 12 August in the Gulf of Maine downwind of the northeastern United States. Details on the locations and meteorological conditions encountered are described by *Fehsenfeld et al.* [2006]

[32] In brief, *RHB* covered predominantly the region of the Gulf of Maine, (42–45)°N, (66–71)°W, whereas the *WP-3* had an extended range, with latitudes between 28°N and 53°N and longitudes between 59°W and 85°W. Temperatures encountered on *RHB* averaged 290 K with a standard deviation (1σ) of 3 K. On the *WP-3*, the temperature range encountered averaged (286 ± 9) K. The pressures on *RHB* were nearly constant at (1012 ± 5) mbar. Because of the altitude range of the *WP-3*, the pressures ranged between 465 and 1023 mbar and averaged to (836 ± 147) mbar.

[33] Figure 8 shows data from the aircraft and the ship on 28 July. At times when aircraft and ship were closer than 30 km together, highlighted by the gray shaded areas, similar photolysis rates were measured. This day also showed some of the highest NO_3 photolysis rates measured

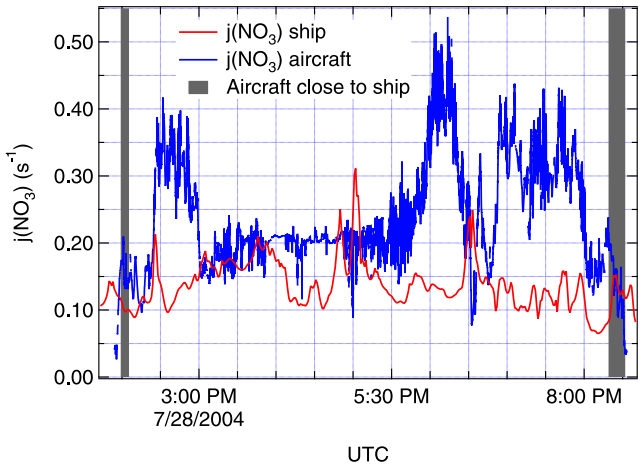

Figure 8. $j(NO_3)$ measurements on *WP-3* (solid curve) and *RHB* (dotted curve) on 28 July 2004. Vertically shaded areas indicate distance *WP-3* ↔ *RHB* < 30 km. These data were collected at latitudes between 42 and 43°N, longitudes between 70 and 71°W and aircraft altitudes below 1000 m. Local time = UTC − 4 hours.

on the *WP-3* during the entire campaign. Around 1800 UTC, the aircraft was flying at high altitude over clouds, the photolysis rates were enhanced strongly because of the large contribution from upwelling radiation caused by cloud reflection.

[34] Figure 9 shows a correlation of simultaneous measurements of downwelling $j(NO_3)$ of the filter radiometers on the ship with the spectroradiometers on the aircraft for the entire ICARTT campaign. The correlation points were taken whenever aircraft and ship were closer together than 0.1 degrees of combined latitude and longitude (about 15 km) and the aircraft altitude was below 1000 m. The correlation at low light conditions (full points) is excellent. At higher light conditions, the measurements were strongly influenced by the aircraft altitude and local cloud effects. For example, the three data points (open markers) to the right of the 1:1 correlation were measured in fog onboard the ship, and over the fog on the airplane. Therefore the aircraft j-values were about a factor of two higher. Overall, this field intercomparison shows general agreement between filter and spectroradiometers.

[35] The quality of the intercomparison stands in contrast to the nadir head intercomparison. A scaling factor to accurately estimate the upwelling radiation from the ocean for $j(NO_3)$ was developed from aircraft measurements meeting four criteria: (1) The aircraft was over the ocean at altitudes below 300 m; (2) the roll angle was under 5°; (3) the actinic flux at 680 nm was above 10^{14} photons cm^{-2} nm^{-1} s^{-1}, to indicate daytime conditions; and (4) the upwelling radiation at 680 nm was less than 15% of the downwelling radiation to exclude measurements taken over clouds or fog. The latter criterion was chosen from close examination of the ratio between upwelling and downwelling radiation. The distribution of this ratio showed two populations of values separated at the 15% ratio, either taken over the clear ocean or over fog, haze, or clouds. After selecting $j(NO_3)$ values meeting all 4 criteria, an average ratio of 0.10 ± 0.03 of upward to downward welling photolysis rates was calculated. This value is quite different from the average value of 0.27 ± 0.06 from the filter radiometers mounted on the ship. The reason for this discrepancy is the mounting position of the nadir head on the ship, which was strongly affected by reflections from the white surface of the ship. Therefore the value of 0.10 from the airborne measurements was used in this study to calculate total NO_3 photolysis rates from the ship by multiplying the downward welling photolysis rates by 1.1. An additional uncertainty of 3% was assigned to these values (see Table 2). This correction is appropriate for the general description of NO_3 photolysis rates in the local MBL; when the measured $j(NO_3)$ is applied to modeling of gas phase measurements made aboard the *RHB*, the residence time of the sampled air parcel over the ship should be significantly shorter than the photolytic lifetime of the compound measured, here NO_3. The maximum fetch over the ship for sampled air (±90° from the ship's bow) is 20 m; at a relative wind speed of 10 m s^{-1} (typical for ICARTT 2004), the sampled air would have been influenced by the local upwelling flux for up to 2 s. Therefore care should be used to account for these effects in such cases.

4.2. Branching Ratio of NO_3 Photodissociation Channels Determined From Field Measurements

[36] The available data from the spectroradiometers allow an investigation of the atmospheric fate of NO_3 due to photolysis channels (R2) and (R3). This branching ratio is not equal to the relative quantum yields of NO_3 photolysis, since the atmospheric actinic flux is not constant in the photolysis wavelength region. Only an actual atmospheric measurement can give insights on how NO_3 photolysis branches into the two channels. Figure 10 shows a scatterplot of $j_{NO}(NO_3)$ versus $j(NO_3)$. A linear fit through the data gives a slope of 0.108. The uncertainty of this value can be estimated by the FWHM (1σ) of a Gaussian fit to a histogram of the ratio of these two photolysis rates. An uncertainty of 0.004 (3.7%) was derived from the histogram shown in Figure 11. In addition to this uncertainty, we include a stated uncertainty of 10% calculated in a previous study due to wavelength uncertainties of the thresholds for NO and NO_2 production [*Johnston et al.*, 1996]. Our

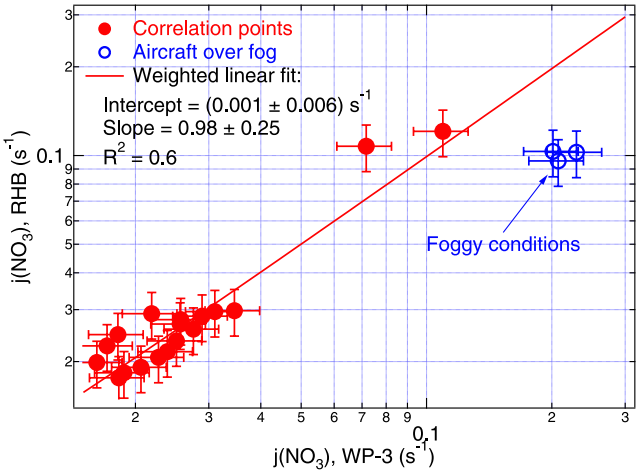

Figure 9. Correlation of ship and aircraft photolysis rates measured when ship and aircraft were within 0.1° of each other and aircraft was below 1000 m.

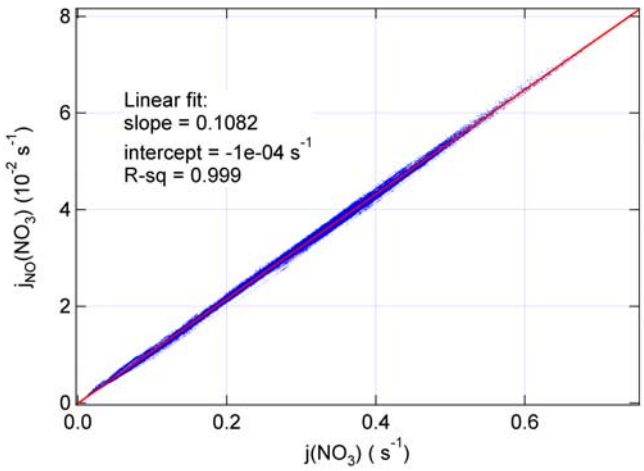

Figure 10. Scatterplot of $j_{NO}(NO_3)$ versus $j(NO_3)$, complete data set from ICARTT 2004 aircraft campaign.

branching ratio of (10.8 ± 1.2)% for NO production versus total NO_3 photolysis is slightly lower than a previous evaluation of (11.4 ± 1.1)% based on stratospheric irradiance measurements by *Johnston et al.* [1996]. The higher ratio of visible light to total radiation in the troposphere compared to the stratosphere explains this difference

4.3. Importance of NO_3 Photolysis in the Marine Boundary Layer and in the Free Troposphere

[37] Our measurements made during ICARTT 2004 on board *RHB* and *WP-3* allow us to assess the importance of NO_3 photolysis during daytime. At these conditions, the only other known significant NO_3 sink is the reaction of NO_3 with NO, with a temperature-dependent rate coefficient [*Sander et al.*, 2003] of

$$k_L(NO_3 + NO) = 1.5 \times 10^{-11} \exp(170\ K/T) cm^3\ molecule^{-1} s^{-1}. \quad (5)$$

[38] We used measured NO mixing ratios, temperatures, and pressures from ship and aircraft to calculate pseudo-first-order loss rate coefficients for NO_3 from

$$k'(NO_3 + NO) = k_L(NO_3 + NO) \times [NO], \quad (6)$$

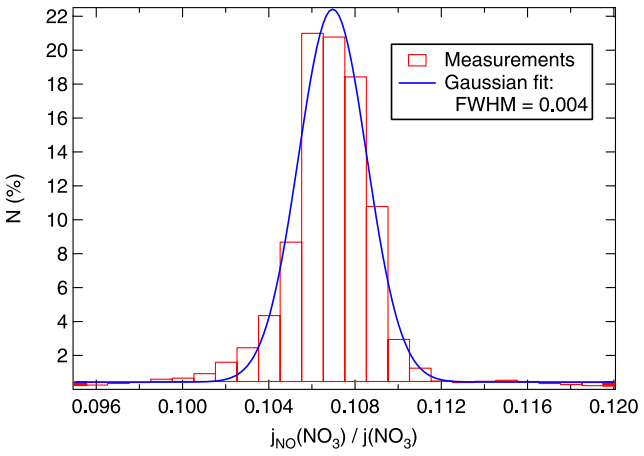

Figure 11. Histogram of $j_{NO}(NO_3)/j(NO_3)$ (bars). Gaussian fit (curve) yields FWHM of 0.004.

which can be directly compared to NO_3 photolysis rates $j(NO_3)$.

[39] Figure 12 shows histograms of those two dominant NO_3 loss rate coefficients for all ship and all aircraft data. Photolysis rates encountered during the day on airplane and ship were of the same magnitude with modes around 0.2 s^{-1}. On the ship in the marine boundary layer (MBL) operating close to the New England coast, both loss processes were important and reaction with NO often dominated. Note that all data influenced by the *RHB* ship exhaust were removed from the data set. On board the aircraft, in the lower and the free troposphere (LT/FT), NO_3 photolysis was the dominant loss process in most sampled air parcels.

[40] However, these loss rate coefficients do not represent the total amount of NO_3 lost to the respective processes, since the NO_3 concentration strongly correlates with the NO concentration. The total NO_3 loss in each sampled air parcel can be calculated by assuming steady state, which will be valid under the rapid daytime loss conditions:

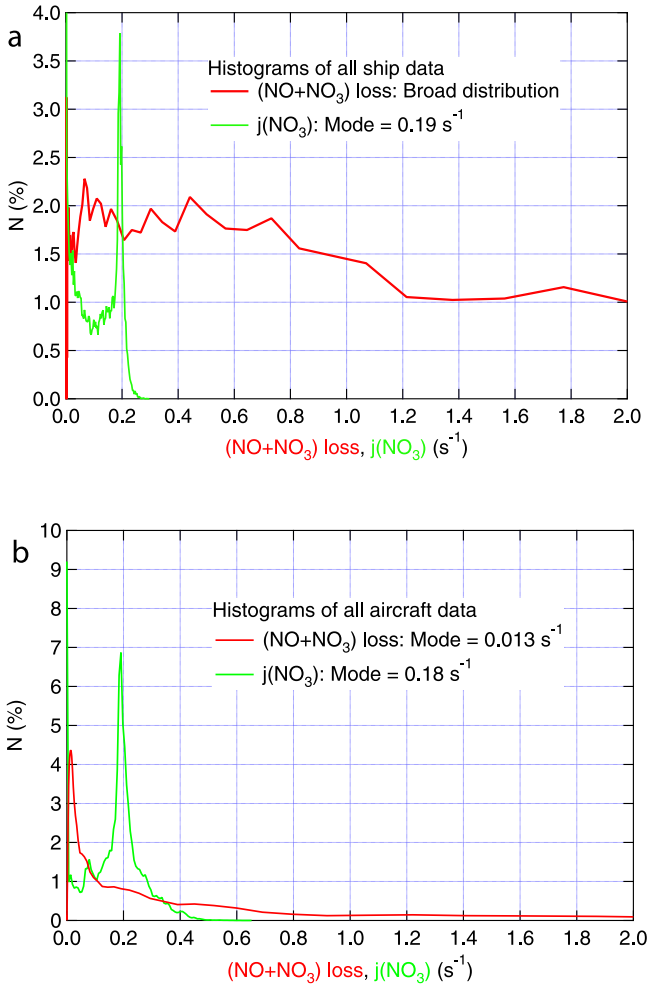

Figure 12. Histograms of (a) ship and (b) aircraft data. Solid curve indicates $j(NO_3)$, and red/dotted curve indicates NO + NO_3 pseudo-first-order loss rate coefficient. Note that for ship data the histogram for NO + NO_3 extends farther to the right, and about 7% of the values are larger than 2 s^{-1}.

Table 3. Average NO_3 Loss Rates for ICARTT 2004 From Ship (*RHB*) and Airplane (*WP-3*)

	NO_3 Photolysis, %	NO_3 + NO, %	Total NO_3 Loss Rate, 10^5 molecules cm^{-3} s^{-1}
WP-3	34	66	4.3
RHB	17	83	19

$$\frac{d[NO_3]}{dt} = -j \cdot [NO_3] - k_L \cdot [NO] \cdot [NO_3] + k_p \cdot [NO_2][O_3] = 0 \quad (7)$$

Rearrangement of this equation allows calculation of the absolute NO_3 loss for each of the two dominant loss processes, when the measured NO_2 and O_3 mixing ratios are included:

$$j \cdot [NO_3] = \frac{j}{j + k_L \cdot [NO]} \cdot k_p \cdot [NO_2] \cdot [O_3], \quad (8)$$

and

$$k_L \cdot [NO] \cdot [NO_3] = \frac{k_L \cdot [NO]}{j + k_L \cdot [NO]} \cdot k_p \cdot [NO_2] \cdot [O_3] \quad (9)$$

Table 3 shows the average of the results of these calculations for both ship and aircraft. In the marine boundary layer sampled by the ship, about one sixth of the NO_3 molecules were photolyzed, in comparison to about one third in the air sampled by the airplane. The total NO_3 loss in the marine boundary layer was about a factor of 4.5 times higher than in the air sampled by the airplane. This discussion indicates that NO_3 photolysis rates are typically higher than loss rates of reaction with NO throughout the troposphere; however, because of the high spatial correlation of NO_3 with NO, actual NO_3 losses due to reaction with NO are higher than photolytic losses in all regions encountered during ICARTT 2004. In other words, the reason for the dominance of NO_3 loss by reaction with NO is based on the fact that both NO and NO_3 are mainly present in polluted air masses. It should be noted that the ship operated primarily in the Gulf of Maine, where marine air is frequently influenced by continental outflow, and that the airplane was frequently aimed at polluted air masses rather than clean air. However, NO mixing ratios encountered on the airplane were generally low showing a lognormal distribution with a main mode at 0.02 ppbv.

4.4. Catalytic Ozone Destruction by NO_3 Photolysis

[41] As outlined in a recent publication by *Brown et al.* [2005], one difference between NO_3 photolysis and reaction with NO is that NO_3 photolysis to yield NO (R2) leads to catalytic ozone destruction:

$$NO_3 + h\nu \rightarrow NO + O_2$$

$$\text{(R4)} \qquad NO + O_3 \rightarrow NO_2 + O_2$$

$$\text{(R5)} \qquad NO_2 + O_3 \rightarrow NO_3 + O_2$$

$$\text{(R6)} \qquad \text{Net}: 2\ O_3 \rightarrow 3\ O_2$$

Combining the data sets during ICARTT 2004 from both platforms gives a broad distribution of O_3 destruction rates up to 70 pptv/hr on the ship and 50 pptv/hr over land on the airplane. Median values for these two platforms were 7.4 pptv/hr and 3.0 pptv/hr, for ship and aircraft, respectively. These values can be compared to typical O_3 uptake rates of 800 pptv/hr over sea and 500 pptv/hr over land, calculated from dry deposition velocities from *Hauglustaine et al.* [1994] and typical boundary layer heights encountered during ICARTT 2004. On average, catalytic ozone destruction during ICARTT 2004 was negligible. However, infrequently it contributed to O_3 loss as high as 8% over sea and 17% over land in the planetary boundary layer (PBL).

[42] *Brown et al.* [2005] reported an upper limit of 10% for the contribution of ozone loss by NO_3 photolysis relative to total ozone loss in certain cases, with the majority of the contributions being below 1% from *WP-3* data during ICARTT 2004. Our combined aircraft and ship data confirm these average numbers, but show that NO_3 photolysis can occasionally enhance O_3 loss by up to 17% in the PBL. A study investigating daytime NO_3 on the ship gives more details on the importance of this process [*Osthoff et al.*, 2006].

5. Summary

[43] We constructed and calibrated spectroradiometers and filter radiometers for the measurement of atmospheric photolysis rates of NO_3 and other compounds. Uncertainties for NO_3 photolysis rates measured in the field were 9% for the spectroradiometers and 14% for the filter radiometers. We determined a detection limit of 10^{-5} s^{-1} for NO_3 photolysis for both instruments sets. We successfully deployed the spectroradiometers on board the NOAA research aircraft *WP-3* and the filter radiometers on board the NOAA research vessel *Ronald H. Brown* during ICARTT in 2004. A field intercomparison on limited occasions during ICARTT showed general agreement between $j(NO_3)$ measured on board the *WP-3* and the *Ronald H. Brown*. Aircraft data measured at low altitudes over the ocean were used to derive an average value of (0.10±0.03) for the ratio of upwelling to downwelling $j(NO_3)$. Our measurements of the atmospheric NO_3 branching ratio of (10.8 ± 1.2)% to form NO from NO_3 photolysis expanded this value to the troposphere. The $j(NO_3)$ measurements in the marine boundary layer (MBL) on board the ship and in the lower and free troposphere (LT/FT) on board the aircraft, in combination with NO_x and O_3 measurements, showed that, because of the close spatial correlation of NO_3 with NO, reaction with NO was more important than photolysis for daytime NO_3 loss during ICARTT 2004. Finally, we concluded that NO_3 photolysis did not contribute significantly

to catalytic destruction of tropospheric ozone both in the MBL and the LT/FT regions.

[44] **Acknowledgments.** We would like to thank the crew of the NOAA research vessel *Ronald H. Brown* and the NOAA Aircraft Operations Center for their support during the field deployment of the instruments during ICARTT 2004. We would also like to thank the Cooperative Institute for Research in Environmental Sciences (CIRES) for their financial support. Parts of this study were financed by the Climate Change and Air Quality Programs of NOAA.

References

Atkinson, R., et al. (1997), Evaluated kinetic, photochemical and heterogeneous data for atmospheric chemistry. 5. IUPAC Subcommittee on Gas Kinetic Data Evaluation for Atmospheric Chemistry, *J. Phys. Chem. Ref. Data*, *26*, 521–1011.

Bohn, B. (2006), Solar spectral actinic flux and photolysis frequency measurements in a deciduous forest, *J. Geophys. Res.*, *111*, D12303, doi:10.1029/2005JD006856.

Brown, S. S., et al. (2001), In situ measurement of atmospheric NO_3 and N_2O_5 via cavity ring-down spectroscopy, *Geophys. Res. Lett.*, *28*, 3227–3230.

Brown, S. S., et al. (2005), Aircraft observations of daytime NO_3 and N_2O_5 and their implications for tropospheric chemistry, *J. Photochem. Photobiol. A Chem.*, *176*, 270–278.

Delbouille, L., et al (1973), *Photometric Atlas of the Solar Spectrum from 3000Å to 10000Å*, Inst. d'Astrophys. de l'Univ. de Liege, Cointe-Ougre, Liege, Belgium.

DeMore, W. B., et al (1997), Chemical kinetics and photochemical data for use in stratospheric modeling, *JPL Publ. 97-4*, Jet Propul. Lab., Pasadena, Calif.

Edwards, G. D., and P. S. Monks (2003), Performance of a single-monochromator diode array spectroradiometer for the determination of actinic flux and atmospheric photolysis frequencies, *J. Geophys. Res.*, *108*(D16), 8546, doi:10.1029/2002JD002844.

Fehsenfeld, F. C., et al. (2006), International Consortium for Atmospheric Research on Transport and Transformation (ICARTT): North America to Europe—Overview of the 2004 summer field study, *J. Geophys. Res.*, *111*, D23S01, doi:10.1029/2006JD007829.

Gardner, E. P., et al. (1987), Primary quantum yields of NO_2 photodissociation, *J. Geophys. Res.*, *92*, 6642–6652.

Geyer, A., et al. (2003), Direct observations of daytime NO_3: Implications for urban boundary layer chemistry, *J. Geophys. Res.*, *108*(D12), 4368, doi:10.1029/2002JD002967.

Gierczak, T., et al. (1997), Atmospheric fate of methyl vinyl ketone and methacrolein, *J. Photochem. Photobiol. A Chem.*, *110*, 1–10.

Harrison, N. J., et al. (2000), Evaluation of spectral irradiance transfer standards, *Metrologia*, *37*, 453–456.

Hauglustaine, D. A., et al. (1994), The importance of atmospheric chemistry in the calculation of radiative forcing on the climate system, *J. Geophys. Res.*, *99*, 1173–1186.

Hofzumahaus, A. (2006), Measurement of photolysis frequencies in the atmosphere, in *Analytical Techniques for Atmospheric Measurement*, edited by D. E. Heard, pp. 406–500, Blackwell, Malden, Mass.

Hofzumahaus, A., et al. (1999), Solar actinic flux spectroradiometry: A technique for measuring photolysis frequencies in the atmosphere, *Appl. Opt.*, *38*, 4443–4460.

Hofzumahaus, A., et al. (2002), Solar actinic radiation (280–420 nm) in the cloud-free troposphere between ground and 12 km altitude: Measurements and model results, *J. Geophys. Res.*, *107*(D18), 8139, doi:10.1029/2001JD900142.

Horowitz, A., et al. (1982), Primary processes in the photolysis of acetaldehyde at 3000 Å and 25°C, *J. Phys. Chem.*, *86*, 3094–3105.

Jakel, E., et al. (2005), Airborne system for fast measurements of upwelling and downwelling spectral actinic flux densities, *Appl. Opt.*, *44*, 434–444.

Johnston, H. S., et al. (1996), NO_3 photolysis product channels: Quantum yields from observed energy thresholds, *J. Phys. Chem.*, *100*, 4713–4723.

Junkermann, W., et al. (1989), A photoelectric detector for the measurement of photolysis frequencies of ozone and other atmospheric molecules, *J. Atmos. Chem.*, *8*, 203–227.

Magnotta, F., and H. S. Johnston (1980), Photo-dissociation quantum yields for the NO_3 free-radical, *Geophys. Res. Lett.*, *7*, 769–772.

Martinez, R. D., et al. (1992), The near UV absorption-spectra of several aliphatic-aldehydes and ketones at 300-K, *Atmos. Environ., Part A*, *26*, 785–792.

McKeen, S. A., et al. (1997), The photochemistry of acetone in the upper troposphere: A source of odd-hydrogen radicals, *Geophys. Res. Lett.*, *24*, 3177–3180.

Meller, R., and G. K. Moortgat (2000), Temperature dependence of the absorption cross sections of formaldehyde between 223 and 323 K in the wavelength range 225–375 nm, *J. Geophys. Res.*, *105*, 7089–7101.

Meller, R., et al. (1991), The UV-visible absorption-spectrum of methylglyoxal, *J. Photochem. Photobiol. A Chem.*, *62*, 163–171.

Osthoff, H. D., et al. (2006), Observation of daytime N_2O_5 in the marine boundary layer during New England Air Quality Study–Intercontinental Transport and Chemical Transformation 2004, *J. Geophys. Res.*, *111*, D23S14, doi:10.1029/2006JD007593.

Sander, S. P., et al (2003), Chemical kinetics and photochemical data for use in atmospheric studies, *JPL Publ. 02-25*, Jet Propul. Lab., Pasadena, Calif.

Sander, S. P., et al (2006), Chemical kinetics and photochemical data for use in atmospheric studies, evaluation number 15, *JPL Publ. 06-02*, Jet Propul. Lab., Pasadena, Calif.

Shetter, R. E., and M. Muller (1999), Photolysis frequency measurements using actinic flux spectroradiometry during the PEM-Tropics mission: Instrumentation description and some results, *J. Geophys. Res.*, *104*, 5647–5661.

Simpson, W. R. (2003), Continuous wave cavity ring-down spectroscopy applied to in situ detection of dinitrogen pentoxide (N_2O_5), *Rev. Sci. Instrum.*, *74*, 3442–3452.

Staffelbach, T. A., et al. (1995), The UV-visible absorption-spectrum and photolysis quantum yields of methylglyoxal, *J. Geophys. Res.*, *100*, 14,189–14,198.

Talukdar, R. K., et al. (1995), Investigation of the loss processes for peroxyacetyl nitrate in the atmosphere: UV photolysis and reaction with OH, *J. Geophys. Res.*, *100*, 14,163–14,173.

Volz-Thomas, A., et al. (1996), Airborne measurements of the photolysis frequency of NO_2, *J. Geophys. Res.*, *101*, 18,613–18,627.

Wayne, R. P., et al. (1991), The nitrate radical—Physics, chemistry, and the atmosphere, *Atmos. Environ., Part A*, *25*, 1–203.

Winer, A. M., et al. (1984), Gaseous nitrate radical—Possible nighttime atmospheric sink for biogenic organic-compounds, *Science*, *224*, 156–159.

Wood, E. C., et al. (2005), Measurements of N_2O_5, NO_2, and O_3 east of the San Francisco Bay, *Atmos. Chem. Phys.*, *5*, 483–491.

F. C. Fehsenfeld, R. Jakoubek, B. M. Lerner, D. D. Parrish, T. B. Ryerson, H. Stark, D. T. Sueper, and E. J. Williams, Chemical Sciences Division, Earth System Research Laboratory, NOAA, 325 Broadway, Boulder, CO 80305, USA. (harald.stark@noaa.gov)

R. Schmitt, Metcon, Inc., 4450 Arapahoe Avenue, Boulder, CO 80303, USA.